

# Photonic Crystal Architecture for Room Temperature Equilibrium Bose-Einstein Condensation of Exciton-Polaritons

Jian-Hua Jiang<sup>1</sup> and Sajeew John<sup>1,2</sup>

<sup>1</sup>*Department of Physics, University of Toronto, Toronto, Ontario, M5S 1A7 Canada*

<sup>2</sup>*Department of Physics, King Abdulaziz University, Jeddah, Saudi Arabia*

(Dated: September 13, 2018)

We describe photonic crystal microcavities with very strong light-matter interaction to realize room-temperature, equilibrium, exciton-polariton Bose-Einstein condensation (BEC). This is achieved through a careful balance between strong light-trapping in a photonic band gap (PBG) and large exciton density enabled by a multiple quantum-well (QW) structure with moderate dielectric constant. This enables the formation of long-lived, dense  $10\ \mu\text{m} - 1\ \text{cm}$  scale cloud of exciton-polaritons with vacuum Rabi splitting (VRS) that is roughly 7% of the bare exciton recombination energy. We introduce a woodpile photonic crystal made of  $\text{Cd}_{0.6}\text{Mg}_{0.4}\text{Te}$  with a 3D PBG of 9.2% (gap to central frequency ratio) that strongly focuses a planar guided optical field on CdTe QWs in the cavity. For 3 nm QWs with 5 nm barrier width the exciton-photon coupling can be as large as  $\hbar\Omega = 55\ \text{meV}$  (i.e., vacuum Rabi splitting  $2\hbar\Omega = 110\ \text{meV}$ ). The exciton recombination energy of 1.65 eV corresponds to an optical wavelength of 750 nm. For  $N = 106$  QWs embedded in the cavity the collective exciton-photon coupling per QW,  $\hbar\Omega/\sqrt{N} = 5.4\ \text{meV}$ , is much larger than state-of-the-art value of 3.3 meV, for CdTe Fabry-Pérot microcavity. The maximum BEC temperature is limited by the depth of the dispersion minimum for the lower polariton branch, over which the polariton has a small effective mass  $\sim 10^{-5}m_0$  where  $m_0$  is the electron mass in vacuum. By detuning the bare exciton recombination energy above the planar guided optical mode, a larger dispersion depth is achieved, enabling room-temperature BEC. The BEC transition temperature ranges as high as 500 K when the polariton density per QW is increased to  $(11a_B)^{-2}$  where  $a_B \simeq 3.5\ \text{nm}$  is the exciton Bohr radius and the exciton-cavity detuning is increased to 30 meV. A high quality PBG can suppress exciton radiative decay and enhance the polariton lifetime to beyond 150 ps at room temperature, sufficient for thermal equilibrium BEC.

## I. INTRODUCTION

Semiconductor microcavities offer an unique platform to study fundamental phenomena of quantum electrodynamics in the strong coupling regime[1–3]. Thanks to advances in growth and manipulation technologies, both excitons and cavity photons are tunable in a variety of ways which enable observations of novel phenomena[3–5]. In the last decade non-equilibrium exciton-polariton BEC have been observed in 1D Fabry-Pérot microcavities in various materials[4–9]. However, polariton lifetime is often too short to achieve thermal equilibrium BEC. Moreover, the BEC temperature is limited by the weakness of photon confinement and the resulting insufficient exciton-photon coupling strength.

In an optical cavity, an atomic excitation and a photon may couple together to form a coherent superposition when their decay rates (times  $\hbar$ ) are much smaller than their coupling. In a semiconductor microcavity[1–3], excitons and photons constitute polaritons in this manner. The quantum superposition of excitons and photons confers them with remarkable dynamics. For instance, the polariton effective mass, inherited from the cavity photon, is about  $10^{-10}$  times the mass of Rubidium atom. Consequently, the BEC transition temperature of polariton gases is usually above 1 K. In the last decade signatures of non-equilibrium polariton BEC has been reported in semiconductor microcavities[4–9]. Although aspects of macroscopic coherence and superflu-

idity have been observed/claimed[6, 10–13], the polariton lifetime has been too short (about 1 ps) to achieve genuine thermal equilibrium[14]. Recently high-quality-factor Fabry-Pérot microcavities have provided longer polariton lifetime[15]. Nevertheless, polaritons can radiatively decay into extraneous and degenerate optical modes of these 1D periodic structures from a micron-scale confinement region.

Due to the half-photon and half-exciton nature of the polariton, the Bose condensate contains polariton-polariton interactions (i.e., optical non-linearity). Such a nonlinear, coherent light source has potential application as a laser with low excitation threshold and novel photon statistics[6, 7, 16–18]. Nonlinearity can also be exploited for the development of all-optical transistors[19], diodes[20], and switches[21, 22]. Unfortunately, most realizations of polariton BEC have been at cryogenic temperatures. Above room-temperature polariton BEC[23] is essential for broad practical applications. While studies on GaN[24], ZnO[25, 26], and organic materials[27] have found room-temperature polariton light emission and lasing, these are not sufficiently long-lived for equilibrium BEC. These room temperature effects are facilitated by large exciton binding energy  $E_b$  and exciton-photon coupling  $\hbar\Omega$ . With small exciton Bohr radius  $a_B$ , the saturation density  $\simeq (5a_B)^{-2}$  at which electron-hole pairs unbind due to many-body effects (screening and phase-space filling as revealed in Ref. [28]) is likewise very high in these materials. On the other hand, small excitons

are very sensitive to local disorder. This leads to strong inhomogeneous broadening that smears the exciton and polariton dispersion. The inhomogeneous broadening in the polymer material measured from optical spectroscopy in Ref. [27] is as high as 60 meV while the exciton-photon coupling is  $\hbar\Omega = 58$  meV. The inhomogeneous broadening in GaN and ZnO are around 16 meV[29] and 25 meV[30], respectively, while the exciton-photon coupling are 25 meV[31] and 29 meV[32], respectively. In contrast the inhomogeneous broadening in GaAs and CdTe is around 1 meV[33]. Nevertheless the exciton-polariton lifetime is still below 1 ps[26] in these materials due to the nature of the optical cavity utilized. Recently, macroscopic occupation of photonic states in microcavities filled with dye molecules has been observed at room temperature[34, 35]. This quasi-condensate[36] in the weak-coupling regime exhibits strongly fluctuating photon number[35], unlike BEC of polaritons in the strong-coupling regime with conserved particle number[4].

In this article, we introduce an alternative approach, using 3D PBG[37, 38] based microcavities[39–41] to greatly enhance the exciton-photon coupling and eliminate radiative decay of polaritons. We focus on CdTe based photonic crystal microcavities since these offer an effective balance between strong light confinement and high exciton density. The exciton binding energy in CdTe QWs has been measured to be about 20 meV (varying with QW width, temperature, etc)[42–44] leading to an exciton Bohr radius  $a_B$  about 4 nm. An exciton-photon coupling of  $\hbar\Omega = 13$  meV has been experimentally realized in CdTe based Fabry-Pérot microcavities with  $N = 16$  QWs[8]. These data indicate that neither the exciton binding energy nor the exciton-photon coupling in CdTe structures is greater than room temperature  $k_B T = 26$  meV. Bare excitons in CdTe QWs are not stable at room temperature and the polariton BEC temperature is below room temperature in Fabry-Pérot microcavities. Indeed non-equilibrium polariton BEC in a CdTe based Fabry-Pérot microcavity is only 19 K[8]. On the other hand, the refractive index of CdTe is sufficient for much stronger light-trapping in the form of 3D PBG. Here we show that using a PBG architecture, the photonic field is much more strongly focused on suitably placed QWs. Consequently, the exciton-photon coupling is enhanced beyond 50 meV (i.e., vacuum Rabi splitting beyond 100 meV). This stabilizes the exciton-polariton and enables equilibrium BEC above room temperature.

For excitons in CdTe multiple QWs (MQWs) with width 3 nm and barrier width 5 nm, the exciton recombination energy is 1.65 eV (optical wavelength 750 nm) and the exciton binding energy is calculated by the effective mass approximation[45] to be 23 meV (larger than the 9 meV in GaAs QW of the same width[46]). The exciton Bohr radius of 3.5 nm is likewise smaller than the corresponding radius in GaAs (8.4 nm)[46], but larger than in ZnO (1.4 nm) and GaN (2.8 nm)[47]. These properties of CdTe lead to stronger coupling, higher saturation density, and stronger thermal stability of excitons

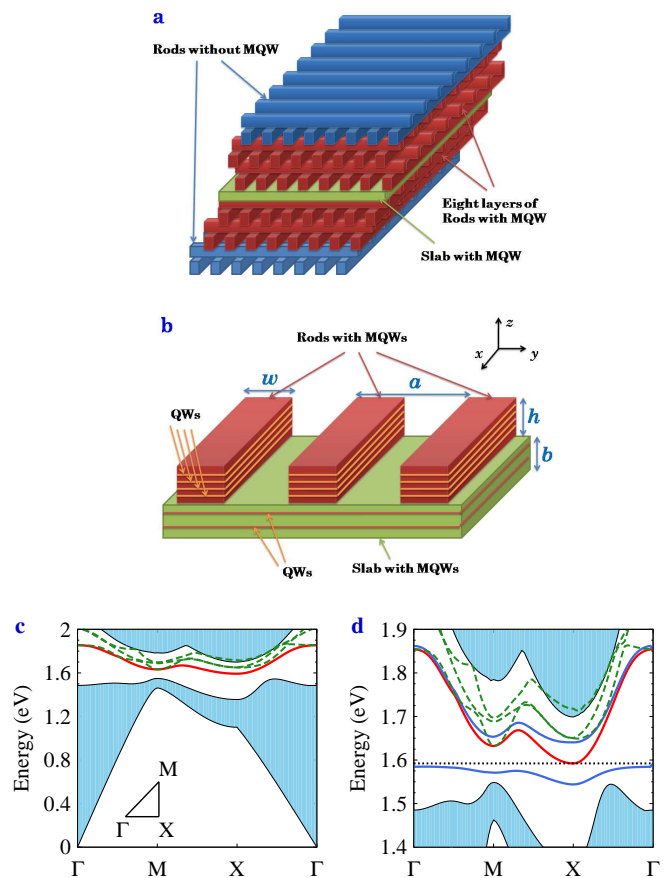


FIG. 1. Photonic crystal architecture and photonic band dispersion. (a) A slab layer sandwiched between two woodpile photonic crystals induces 2D photonic bands (“guided modes”) in the 3D PBG with  $\delta\omega/\omega_c = 9.2\%$  where  $\delta\omega$  is band gap width and  $\omega_c$  is the PBG central frequency. (b) QWs are grown in the slab and the eight nearby layers of rods. Typically  $a \simeq 360$  nm,  $w = 0.25a \simeq 90$  nm,  $h = 0.3a \simeq 110$  nm,  $b = 0.06a \simeq 20$  nm. There are about 100 QWs with the same width. There are two QWs in the slab layer and about 12 QWs in each rod. The QW width is chosen to be 3, 4, 5, 6 nm for comparison, while the width of the barrier layers between QWs is fixed to be 5 nm. QWs are made of CdTe (dielectric constant 8.5) while the barriers and photonic crystals are made of  $\text{Cd}_{0.6}\text{Mg}_{0.4}\text{Te}$  (dielectric constant 7.5). In the regions with QWs, the dielectric constant is taken to be 8 (average of the two materials). (c) and (d) Dispersion of the 2D guided modes (green dashed and red solid curves) and the bulk 3D photonic bands (shaded regions). The first Brillouin zone of the 2D guided modes is  $-\frac{\pi}{a} \leq q_x, q_y < \frac{\pi}{a}$ . The lowest 2D photonic band (the solid curves in (c) and (d)) is coupled with excitons (dotted curve in (d)) in QWs. The lower and upper polariton branches (blue solid curves in (d)) are depicted for exciton recombination in resonance with the lowest 2D guided mode. In this case, each QW width is 4 nm; exciton recombination energy is  $E_{X0} = 1.59$  eV; the photonic lattice constant is chosen to be  $a = 360$  nm. The exciton-photon coupling strength and the on-resonance lower polariton dispersion depth is 48 meV. Larger dispersion depth and higher BEC temperature is achieved by detuning the exciton recombination energy above the lowest 2D guided mode.

compared to GaAs. CdTe is nevertheless suitable for high quality microcavities for which growth technology is well-developed[3, 43]. CdTe has a dielectric constant of 8.5[43, 48, 49] above the threshold for PBG formation. We propose to use  $\text{Cd}_{0.6}\text{Mg}_{0.4}\text{Te}$  as the barriers between QWs as well as for the background photonic crystal. The dielectric constant of  $\text{Cd}_{0.6}\text{Mg}_{0.4}\text{Te}$  is 7.5[50]. This gives a photonic band gap (PBG) in the woodpile architecture (see Fig. 1) of  $\delta\omega/\omega_c = 9.2\%$  ( $\delta\omega$  denotes band gap width and  $\omega_c$  is the PBG central frequency). The dielectric constant of the regions with MQWs is taken to be 8, which is the average value of the QW and barrier materials. Using  $N = 106$  QWs, the exciton-photon coupling is as large as  $\hbar\Omega = 55$  meV, i.e., the vacuum Rabi-splitting is 110 meV. The exciton-photon coupling per QW of  $\hbar\Omega/\sqrt{N} = 5.4$  meV is considerably larger than  $13/\sqrt{16} = 3.3$  meV for the Fabry-Pérot microcavity reported in Ref. [8] (i.e., exciton-photon coupling of 13 meV for 16 QWs). We also calculate the exciton-photon coupling when the number of QWs in each rod is reduced by increasing the barrier width (keeping two QWs in the central slab). The exciton-photon coupling is 45 meV if the barrier width is increased to 10 nm while there are 7 QWs in each rod in the active region (total of 58 QWs). When the barrier width is increased to 20 nm with 4 QWs in each rod in the active region (total 34 QWs), the exciton-photon coupling is 40 meV. If there are only two QWs in the central slab and no QW in the rods, the exciton-photon coupling remains as high as 33 meV. All these energies are greater than room temperature  $k_B T = 26$  meV and (with positive detuning of the exciton recombination energy from the lowest 2D guided mode) are shown below to support room-temperature polariton BEC.

Fabrication of the structure proposed (as shown in Fig. 1a and 1b) is possible using wafer-fusion and laser beam-assisted precise alignment of rods[51, 52]. It has been demonstrated[40] that a layer of rods with MQWs (grown by molecular beam epitaxy and etched) can be placed in a woodpile photonic crystal. By repeated wafer-fusion, laser-assisted alignment, careful etching and polishing (monitored by thin-film interference), sandwich structures can be fabricated with high precision. Accurate fabrication of GaAs woodpile photonic crystals with a near-infrared, MQW, light-emitting layer was reported by Noda *et al.*[40]. Similar techniques can, in principle, be employed for our proposed CdTe photonic crystal structure.

3D photonic crystal microcavities have been fabricated with much higher quality factor than their counterpart Fabry-Pérot microcavities. Quality factors as high as  $2 \times 10^6$  have been demonstrated experimentally for microcavities in the woodpile architecture[53]. In addition, 3D PBG eliminates purely radiative recombination of excitons into unwanted modes when the lower polariton energy is in the PBG. In this case, the polariton lifetime is determined by exciton non-radiative recombination. In CdTe QWs at room temperature, the exciton photolumi-

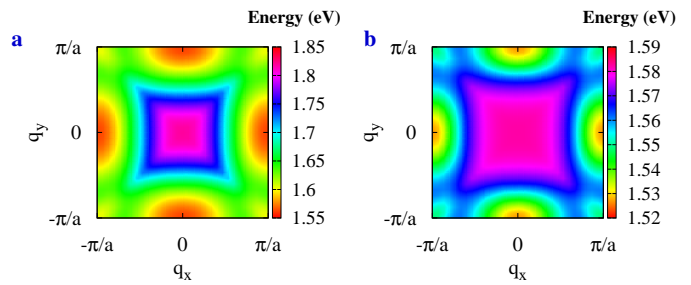


FIG. 2. Dispersion of confined photonic and polaritonic bands in 2D wavevector space. (a) Dispersion of the lowest confined photonic band in the first Brillouin zone  $-\frac{\pi}{a} \leq q_x, q_y < \frac{\pi}{a}$ . The lattice constant is  $a = 365$  nm. (b) Dispersion of the lower polariton branch in the same wavevector region. The QW width is 4 nm. The lower band edge (1.56 eV) of guided 2D modes within the 3D PBG is 30 meV below the excitonic recombination energy ( $E_{X0} = 1.59$  eV). The exciton-photon coupling of 48 meV involves the collective response of 100 QWs.

nescence decay time is measured to be 150 ps in Ref. [54], suggesting that the non-radiative recombination time is even longer. This time scale is sufficient for polaritons to reach thermal equilibrium since the exciton-optical-phonon scattering in CdTe at room temperature is quite efficient[55]. Our calculation reveals that room temperature equilibrium polariton BEC can be achieved for a polariton density of  $5 \times 10^3 \mu\text{m}^{-2}$  (exciton density in each QW of  $\sim (30a_B)^{-2}$ , below the saturation density of  $(5a_B)^{-2}$  where  $a_B = 3.5$  nm is the bare exciton Bohr radius for QW of width 3 nm). This occurs when the exciton recombination energy is detuned 30 meV above the lowest 2D guided mode and the excitons are trapped in a box with side length of  $10\text{-}10^4 \mu\text{m}$ . Realization of equilibrium polariton BEC at and above room temperature may open the door to broad applications of quantum mechanics beyond the microscopic scale.

## II. POLARITONS IN A 3D PHOTONIC BAND GAP MICROCAVITY

Figs. 1a and 1b depict our proposed woodpile photonic crystal heterostructure. The distance between the nearest neighbor rods in the same layer is denoted by  $a$ , the height of each rod is  $h = 0.3a$ , the width of each rod is  $w = 0.25a$ , and the thickness of the solid central slab is  $b = 0.06a$ . In order to place the lowest 2D guided mode within the PBG in resonance with the exciton transition at 1.59 eV (for QW width 4 nm) typically  $a = 360$  nm. The PBG is centered in the range of 750 nm[56]. MQWs are grown in the slab and the eight layers of rods close to the slab. The other regions above and below are the cladding woodpile photonic crystals. The QWs are made of CdTe, while the barrier layers between QWs are made of  $\text{Cd}_{0.6}\text{Mg}_{0.4}\text{Te}$ . Both materials are direct electronic band-gap semicon-

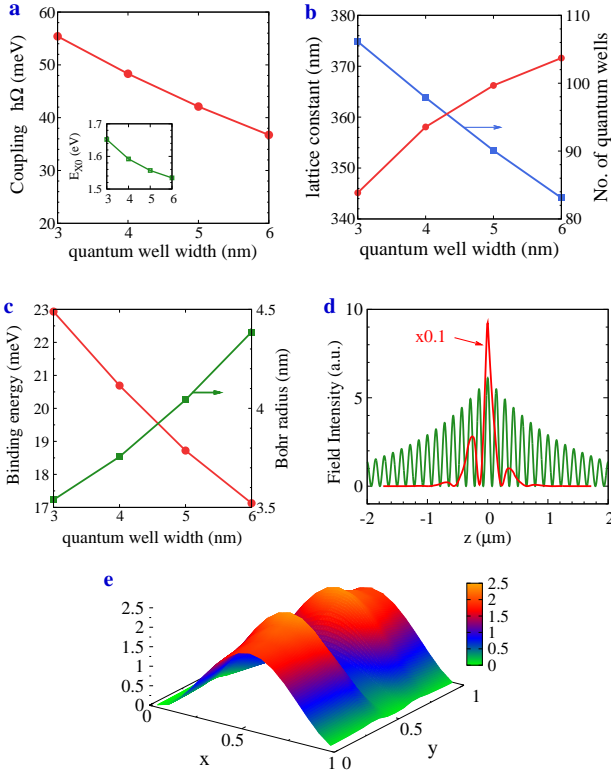


FIG. 3. Very strong light-matter interaction in photonic band gap 2D guided mode. (a) Exciton-photon collective interaction strength  $\hbar\Omega$  as a function of QW width for fixed barrier width of 5 nm. The horizontal axis spans from  $N = 106$  to 83 QWs. Inset: exciton recombination energy  $E_{X0}$ . The lowest 2D photonic band edge  $\hbar\omega_0$  is kept in resonance with the exciton recombination energy  $E_{X0}$  as the QW width is varied. The barrier layers between QWs are made of  $\text{Cd}_{0.6}\text{Mg}_{0.4}\text{Te}$ . (b) As  $E_{X0}$  varies with the QW width, the photonic crystal lattice constant  $a$  is adjusted (red curve) to keep  $\hbar\omega_0 = E_{X0}$ . Since  $a$  changes, the total number  $N$  of QWs (blue curve) in the slab and rods also changes. (c) Exciton binding energy and Bohr radius for different QW widths calculated using effective mass approximation[45] [see Appendix]. (d) Average electric field intensity  $S^{-1} \int d\vec{\rho} |\vec{\mathcal{E}}(\vec{\rho}, z)|^2$  profile at 2D guided mode edge in PBG cavity (red curve) compared to that in  $\text{Cd}_{0.4}\text{Mg}_{0.6}\text{Te}/\text{Cd}_{0.8}\text{Mn}_{0.2}\text{Te}$  Fabry-Pérot cavity[44] (green curve) along the  $z$ -direction. The photons in both cavities have band edge energy, 1.59 eV. The photonic field intensity in the PBG cavity is multiplied by a factor of 0.1 in the figure. The Fabry-Pérot cavity is a  $\lambda/2$  cavity with  $\lambda = 780$  nm. The lattice constant of the photonic crystal is  $a = 360$  nm. (e) Field intensity  $|\vec{\mathcal{E}}|^2$  profile in the  $x$ - $y$  plane (in one unit cell of photonic crystal) at  $z = 0$ . Here the averaged intensity is 1.  $x$  and  $y$  coordinates are in unit of the photonic lattice constant  $a$ .

ductors with band structure similar to GaAs. The electronic band-gaps of CdTe and  $\text{Cd}_{0.6}\text{Mg}_{0.4}\text{Te}$  are 1.475 eV and 2.28 eV, respectively[57, 58] (from linear interpolation between the band gaps of CdTe and MgTe, the latter being 3.49 eV). The cladding rods without QWs are also made of  $\text{Cd}_{0.6}\text{Mg}_{0.4}\text{Te}$ . The structure breaks the trans-

lation symmetry along the  $z$ -direction (see Fig. 1a), but has lattice translation symmetry in the  $x$ - $y$  plane (the coordinate axes are depicted in Fig. 1b). There is no inversion symmetry with respect to the slab. However the system has a  $D_{2d}$  symmetry with two mirror planes: the  $y$ - $z$  and  $x$ - $z$  planes[59]. There are several 2D guided photonic bands localized around the slab. The dispersion of those confined modes within the PBG are shown in Figs. 1c and 1d. The electric field in these 2D bands can be written as:

$$\vec{\mathcal{E}}_{i,\vec{q}}(\vec{r}) = \sqrt{\frac{\hbar\omega_{i,\vec{q}}}{2\varepsilon_0 S}} \vec{u}_{i,\vec{q}}(\vec{r}) e^{i\vec{q}\cdot\vec{\rho}}. \quad (1)$$

Here  $\varepsilon_0$  is the vacuum permittivity,  $S$  is the area of the structure in the  $x$ - $y$  plane,  $\vec{r} = (\vec{\rho}, z)$  with  $\vec{\rho} = (x, y)$ , and  $\omega_{i,\vec{q}}$  is the frequency of a photon in the  $i$ -th band with a Bloch wavevector  $\vec{q}$  in the 2D Brillouin zone  $-\frac{\pi}{a} \leq q_x, q_y < \frac{\pi}{a}$ . The field is normalized such that  $S^{-1} \int d\vec{\rho} dz \varepsilon(\vec{r}) |\vec{u}_{i,\vec{q}}(\vec{r})|^2 = 1$  where  $\varepsilon(\vec{r})$  is the coordinate-dependent dielectric function. Photons in the lowest confined photonic band and electron-heavy-hole excitons in the MQWs interact to form the lower and upper polariton branches. These are depicted in Fig. 1d when the exciton recombination energy coincides with 2D photonic band edge. The dispersion of the lowest confined photonic band and that of the lower polariton branch in the 2D photonic Brillouin are shown in Fig. 2 for the case when the exciton recombination energy is detuned by 30 meV above the 2D photonic band edge.

The energy levels and wavefunctions of the  $1s$  excitonic states in QWs are obtained from diagonalizing the effective mass Hamiltonian[45] [see Appendix for details]. Combining the microscopic details of cavity photons and QW excitons, the Hamiltonian of the coupled exciton-photon system[46] is given by:

$$H = H_X + H_P + H_{int} \quad (2a)$$

$$H_X = \sum_{l,\alpha,n,\vec{q}} E_X^{(l)}(\vec{q} + \vec{G}_n) \beta_{l,\alpha,\vec{q}+\vec{G}_n}^\dagger \beta_{l,\alpha,\vec{q}+\vec{G}_n}, \quad (2b)$$

$$H_P = \sum_{i,\vec{q}} \hbar\omega_{i,\vec{q}} a_{i,\vec{q}}^\dagger a_{i,\vec{q}}, \quad (2c)$$

$$H_{int} = \sum_{l,\alpha,n,i,\vec{q}} i\hbar\bar{\Omega}_{l,\alpha,n,i,\vec{q}} \beta_{l,\alpha,\vec{q}+\vec{G}_n}^\dagger a_{i,\vec{q}} + \text{H.c.} \quad (2d)$$

The operator  $\beta_{l,\alpha,\vec{q}+\vec{G}_n}^\dagger$  creates a  $1s$  exciton in the  $l$ -th QW with polarization  $\alpha = L, T$  (longitudinal or transverse) and center of mass wavevector  $\vec{q} + \vec{G}_n$  where  $\vec{G}_n = \frac{2\pi}{a}(n_x, n_y)$  is the 2D reciprocal lattice vector for the photonic band structure with integers  $n_x$  and  $n_y$ . The exciton dispersion  $E_X^{(l)}(\vec{q}) = E_X(\vec{q}) + \delta E_l$  with  $E_X(\vec{q}) \equiv E_{X0} + \frac{\hbar^2 q^2}{2m_X}$  includes a fluctuation term  $\delta E_l$  varying for different QWs to describe disorder effects.  $E_{X0}$  is the exciton recombination energy at zero center-of-mass wavevector.  $m_X = m_e + m_h$  is the effective mass of exciton with  $m_e$  and  $m_h$  being the electron and hole

effective masses, respectively. The operator  $a_{i,\vec{q}}^\dagger$  creates a photon in the  $i$ -th band with Bloch wavevector  $\vec{q}$ . The coupling matrix element is calculated[46] as:

$$\bar{\Omega}_{l,\alpha,n,i,\vec{q}} = \frac{|\phi(0)|d\sqrt{\omega_{i,\vec{q}}}}{S_{u.c.}\sqrt{2\hbar\varepsilon_0}} \times \int_{u.c.} d\vec{\rho} e^{-i\vec{G}_n \cdot \vec{\rho}} u_{\alpha,i,\vec{q}}(\vec{\rho}, z_l) \Theta(\vec{\rho}, z_l). \quad (3)$$

$|\phi(0)|$  denotes the amplitude of the  $1s$  exciton wavefunction when the distance between electron and hole is zero.  $d$  is the inter-band dipole matrix element in CdTe.  $z_l$  is the coordinate of the center of the  $l$ -th QW in the  $z$ -direction.  $S_{u.c.} = a^2$  is the area of the unit cell in the  $x$ - $y$  plane.  $u_{\alpha,i,\vec{q}} = \vec{e}_\alpha \cdot \vec{u}_{i,\vec{q}}$ , where  $\vec{e}_\alpha$  is an unit vector along the polarization direction of the  $\alpha$  exciton. For longitudinal ( $\alpha = L$ ) excitons  $\vec{e}_\alpha$  is along  $\vec{q}$  while for transverse ( $\alpha = T$ ) exciton it is perpendicular to both  $\vec{q}$  and the  $z$  direction.  $\Theta(\vec{r})$  equals 1 when the coordinate  $\vec{r}$  is in the semiconductor region and 0 when  $\vec{r}$  is in the air region.  $\Theta(\vec{r})$  describes the overlap between the photonic field and the excitonic wavefunction. The integration in Eq. (3) is over the unit cell (u.c.) of the structure in the  $x$ - $y$  plane.

It is sufficient to use only the spectrum close to the energy minima of the lowest confined photonic band to calculate the dispersion of the lower polariton branch (see Figs. 1d and 2b). This branch is essential for the study of polariton BEC. There are two energy minima for the photon: one at  $\vec{Q}^{(x)} = (\frac{\pi}{a}, 0)$ , the other at  $\vec{Q}^{(y)} = (0, \frac{\pi}{a})$ . We consider the situation when the exciton recombination energy  $E_{X0}$  is close to the two energy minima. The photonic dispersion around the two minima is approximately parabolic,

$$\hbar\omega_{\vec{q}} = \hbar\omega_0 + \frac{\hbar^2(q_x - Q_x^{(\nu)})^2}{2m_x^{(\nu)}} + \frac{\hbar^2(q_y - Q_y^{(\nu)})^2}{2m_y^{(\nu)}} \quad (4)$$

with  $\nu = x, y$ . From the  $D_{2d}$  symmetry, the photonic effective masses satisfy the relations  $m_x^{(x)} = m_y^{(y)}$  and  $m_x^{(y)} = m_y^{(x)}$ . If  $a = 360$  nm, plane wave expansion calculation[60] yields  $m_x^{(x)} = 2.9 \times 10^{-5}m_0$  and  $m_x^{(y)} = 4.7 \times 10^{-5}m_0$  where  $m_0$  is the electron mass in vacuum. Scale invariance of the Maxwell equations dictates that  $\omega_0$ ,  $m_x^{(x)}$ , and  $m_y^{(y)}$  are proportional to  $1/a$ . For CdTe QWs, the effective mass of the conduction band electron is  $m_e = 0.095m_0$ [58], while the effective mass of the heavy-hole is  $m_h = 0.4m_0$ [48].

When the fluctuation in the excitation energy among QWs is neglected, i.e.,  $E_X^{(l)}(\vec{q}) = E_X(\vec{q})$  for all  $l$ , we introduce the collective excitonic operator  $b_{\vec{q}} \equiv \sum_{l,\alpha,n} \frac{\Omega_{l,\alpha,n,\vec{q}}}{\Omega_{\vec{q}}} \beta_{l,\alpha,n,\vec{q}}$  to obtain the effective polariton

Hamiltonian[61, 62]:

$$H = H_0 + H_I, \quad (5a)$$

$$H_0 = \sum_{\vec{q}} \left[ E_X(\vec{q}) b_{\vec{q}}^\dagger b_{\vec{q}} + \hbar\omega_{\vec{q}} a_{\vec{q}}^\dagger a_{\vec{q}} \right], \quad (5b)$$

$$H_I = \sum_{\vec{q}} i\hbar\Omega_{\vec{q}} (b_{\vec{q}}^\dagger a_{\vec{q}} - a_{\vec{q}}^\dagger b_{\vec{q}}). \quad (5c)$$

The collective exciton-photon coupling is given by

$$\hbar\Omega_{\vec{q}} = \hbar \sqrt{\sum_{l,\alpha,n} |\bar{\Omega}_{l,\alpha,n,\vec{q}}|^2}. \quad (6)$$

Here  $b_{\vec{q}}$  corresponds to the mode that couples most strongly to the lowest 2D guided mode in the PBG. Other excitonic modes orthogonal to this mode (in the Hilbert space of excitonic states spanning all QWs) are much more weakly coupled to the 2D photonic bands. In the above equations, the photonic band index  $i$  is omitted since only the lowest confined 2D photonic band is relevant. We also approximate the  $\vec{q}$  dependence of the collective coupling by its value at the two polariton energy minima and define  $\Omega \equiv \hbar\Omega_{\vec{Q}^{(x)}} = \hbar\Omega_{\vec{Q}^{(y)}}$ . This is justified since beyond the narrow range around the two energy minima, the lower polariton dispersion becomes exciton-like and its detailed form does not alter the low energy dynamics (see Figs. 1d and 2b). The dispersion of the lower polariton branch is given by

$$E_{LP}(\vec{q}) = \frac{E_X(\vec{q}) + \hbar\omega_{\vec{q}}}{2} - \left[ \left( \frac{E_X(\vec{q}) - \hbar\omega_{\vec{q}}}{2} \right)^2 + \hbar^2\Omega^2 \right]^{\frac{1}{2}}. \quad (7)$$

The above dispersion can likewise be extended to the whole 2D wavevector space since away from the energy minima  $\vec{Q}^{(x)}$  and  $\vec{Q}^{(y)}$ , the dispersion of the lower polariton becomes exciton-like (i.e., almost flat dispersion).

### III. VERY STRONG LIGHT-MATTER INTERACTION

Fig. 3a shows the collective exciton-photon coupling  $\hbar\Omega$  calculated for different QW width when excitons are in resonance with the lowest 2D guided mode for photons, i.e.,  $E_{X0} = \hbar\omega_0$ . The vacuum Rabi splitting,  $2\hbar\Omega$ , exceeds 100 meV when the QW width is 3 nm (experimentally accessible as shown by Refs. [64, 65]). The width of the barrier layers between QWs is fixed at 5 nm throughout this work. Fig. 3b depicts how the photonic crystal lattice constant  $a$  must be adjusted as the QW width is varied, in order to maintain resonance between the exciton recombination energy and the 2D guided mode. The total number of QWs that fit into the active region is correspondingly adjusted. Fig. 3c depicts the variation of the exciton binding energy and Bohr radius with QW width. The calculated exciton binding energies, ranging

from 17 meV to 23 meV, agree well with experimental results of 17 ~ 25 meV[42–44].

Considerable enhancement of the exciton-photon coupling in our photonic crystal microcavity (compared with Fabry-Pérot microcavities) originates from the light-trapping effect of the PBG. In Fig. 3d we compare the photonic field intensity  $|\vec{\mathcal{E}}|^2$  distribution as a function of  $z$ , but averaged over the  $x$ - $y$  plane for the  $\text{Cd}_{0.4}\text{Mg}_{0.6}\text{Te}/\text{Cd}_{0.8}\text{Mn}_{0.2}\text{Te}$  Fabry-Pérot and the 3D photonic crystal microcavities with the same photon energy. The photonic crystal microcavity clearly focuses the electric field much more strongly than the Fabry-Pérot. Moreover the averaged electric field intensity at  $z = 0$  is significant larger. This is because in photonic crystal a large volume fraction ( $\simeq 75\%$ ) is air, which reduces the over all dielectric constant of the structure. The reduced screening enhances the averaged electric field intensity  $|\vec{\mathcal{E}}|^2$  at  $z = 0$  by eight times. Another important advantage of the PBG heterostructure are the strong spatial variations of the field intensity in the  $x$ - $y$  plane. The higher intensity regions act as an attractive “optical potential” for the exciton and the wavefunction of the lower polariton is peaked in these “hot spots”. This offers a way to “pattern” the polariton condensates in the  $x$ - $y$  plane (see Fig. 3e). The peak intensity in the  $x$ - $y$  plane is greater than the average intensity depicted in Fig. 3d. This provides further enhancement in exciton-photon coupling compared to the 1D Fabry-Pérot geometry for which the field intensity is uniform in the  $x$ - $y$  plane. From Figs. 3d and 3e the peak intensity is about 38 times (the average intensity is 16 times) as large as that in the Fabry-Pérot microcavity. Other photonic crystals that have a larger PBG, such as the slanted-pore photonic crystals[66], provide even stronger light focusing and larger exciton-photon couplings than we have presented here using the woodpile architecture.

Another advantage of PBG light-trapping is that the quality factor of the microcavity can be very high. A quality factor of  $2 \times 10^6$  with nanosecond photonic lifetime has been experimentally demonstrated in the woodpile architecture[53]. This quality factor can be further enhanced by simply increasing the thickness of the cladding photonic crystal. Our calculation indicates that moderate fabrication imperfection does not reduce the quality factor considerably due to the existence of the 3D PBG [see the end of next section]. When radiative decay is strongly inhibited, polaritons can decay through slower non-radiative processes. The Auger recombination rate[67] is estimated as about  $10^{-3}$  second [see Appendix]. Non-radiative recombination triggered by electronic impurity states such as the Shockley-Read-Hall mechanism[68], may be more important in polariton decay. Nevertheless, the measured photoluminescence decay time of 150 ps in CdTe QW at room temperature[54] suggests that non-radiative polariton decay time should be longer than 150 ps. The non-radiative exciton decay time is believed to be on the order of nanoseconds[4]. Clearly, very strong exciton-photon coupling, long po-

lariton lifetime, and small polariton effective mass are possible in the photonic crystal microcavity.

#### IV. ROOM TEMPERATURE POLARITON BEC

In this section we delineate the precise conditions for room temperature polariton BEC in our photonic crystal microcavity. The BEC transition temperature is very sensitive to the dispersion depth of the lower polariton branch and the density of polaritons, but relatively insensitive to the polariton trapping area over a broad range of lengths,  $D$ , from 10  $\mu\text{m}$  to 1 cm, when the polariton density is high. The polariton density can be controlled by excitation of electron-hole pairs with energy above the upper 3D photonic band edge. These carriers can then relax into the lower polariton branch within the PBG. Since the polariton lifetime is enhanced beyond the thermalization time (on the order of ps at room temperature), polaritons achieve thermal equilibrium long before they decay. We consider a finite-sized trap with box (square well potential) confinement in the  $x$ - $y$  plane. This square quantum box has a side length of  $D$ . Such a box can be created by replacing our infinite central slab by a finite-sized slab[40, 53, 69] or by increasing the Mg fraction outside the prescribed box region[70] to create a barrier for excitons. Trapping by these means enables higher BEC transition temperature than harmonic trapping potentials induced by strain[18]. The trapping box induces quantization of the polariton wavevector in  $x$  and  $y$  directions, discretizing the polariton spectra, and enabling the BEC phase transition that would otherwise be forbidden in an infinite 2D system. To simplify the calculation we approximate the polariton effective mass with the isotropic “density-of-states mass”  $m_{dos} = \sqrt{m_x^{(x)} m_x^{(y)}}$ .

In Figs. 4a and 4b, we plot the ground state occupation  $N_0$  as a function of the polariton density. The polariton distribution is calculated assuming a non-interacting, equilibrium polariton gas. There is a rapid increase of  $N_0$  around a threshold density, above which  $N_0$  becomes comparable with the total polariton number  $N_{tot}$ . We define the polariton BEC transition according to the criterion  $N_0/N_{tot} = 0.1$ [71] This criterion gives lower estimate of the BEC transition temperature than the criterion employed by Ketterle and van Druten[72]. At low temperatures, polaritons are mainly distributed in the low energy, photon-like states around the bottom of the lower polariton branch with very small effective mass (see Fig. 4c). The small effective mass enhances condensation and reduces the threshold density for polariton BEC. The dispersion depth of these photon-like states is

$$V \equiv (E_X - E_{LP})|_{\vec{q}=0} = \frac{\Delta}{2} + \sqrt{\left(\frac{\Delta}{2}\right)^2 + \hbar^2\Omega^2}, \quad (8)$$

where  $\Delta = E_{X0} - \hbar\omega_0$  is the detuning between the exciton and photon. On the other hand, if the temperature is comparable or higher than  $V/k_B$ , the occupation of high

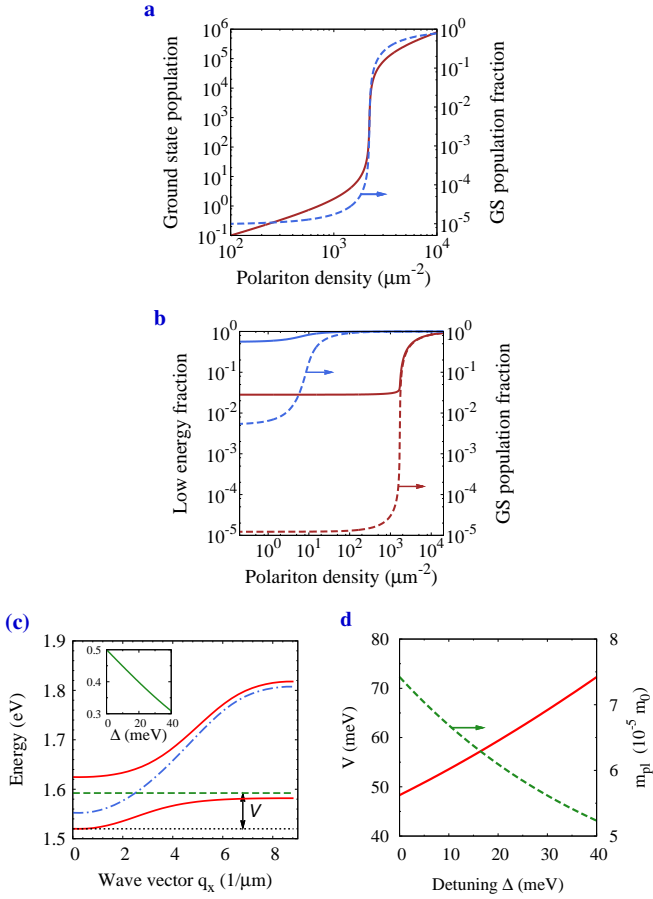


FIG. 4. Polariton population on ground state and other low energy states for exciton box trap with  $D = 10 \mu\text{m}$ , exciton-photon coupling of  $\hbar\Omega = 48$  meV, and exciton recombination energy of  $E_{X0} = 1.59$  eV. The QW width is 4 nm and the barrier layer width is 5 nm. The detuning is  $\Delta = 30$  meV for (a) and  $\Delta = 40$  meV for (b). (a) Population of the ground state (GS) vs. polariton density (solid curve). The rapid, nonlinear increase of GS population indicates the BEC transition. The GS population fraction (dashed curve) i.e. GS population divided by the total population is of order unity for densities beyond the BEC transition. (b) GS population fraction (dashed curves) and the population fraction on the low energy discrete states (solid curves) below the continuum exciton recombination energy  $E_{X0}$  (there are more than 1000 such states). These are photon-like states with very small effective mass, whereas states higher than  $E_{X0}$  are exciton-like. When a large population fraction resides in the photon-like states, the BEC threshold density is reduced. For  $T = 100$  K (blue curves), populated polariton states are mostly photon-like. The threshold density is much lower than for  $T = 300$  K (brown curves) where the population fraction on low energy states is negligible. (c) The dispersion of polaritons (red solid curves), bare exciton (green dashed curve), and pure photon (blue chain) for detuning  $\Delta = 40$  meV. The dispersion depth of the lower polariton branch  $V$  is also depicted (the black dotted line denotes the lower polariton band edge). Inset: excitonic fraction of the lower polariton branch as a function of detuning  $\Delta$ . (d) The dispersion depth  $V$  (red solid curve) and polariton effective mass  $m_{pl}$  (green dashed curve) of the lower polariton branch vs. the detuning  $\Delta$ .

energy, exciton-like states is significant. The effective mass of the bare exciton is around four orders of magnitude larger than the 2D guided photon effective mass. Likewise the density of exciton-like states is about four orders of magnitude larger than the low-energy, photon-like states. The consequences of this are indicated in Figs. 4a (low temperature case) and 4b (high temperature case). Polariton BEC at temperatures comparable with  $V/k_B$  require very high polariton density. Since the polariton is a quantum superposition of a photon and an exciton, the polariton density cannot exceed a specific “saturation density”, beyond which exciton-exciton interaction cause considerable exciton ionization. Therefore, the polariton BEC transition temperature is essentially limited by the dispersion depth  $V$ . The dispersion depth is increased by a positive detuning  $\Delta$  (see Fig. 4d). However, the excitonic fraction of the polariton is reduced with increasing  $\Delta$ . This reduces the phonon-polariton and polariton-polariton interactions and consequently it takes longer time for polaritons to reach their thermal equilibrium. From experimental measurements[55] the phonon-polariton scattering time at room temperature is estimated to be about 0.1 ps [see Appendix]. A thermalization time on the order of 1 ps is possible if the exciton fraction is higher than 10%. In the range of detuning considered in this article,  $0 < \Delta < 40$  meV, the excitonic fraction is greater than 19% for exciton-photon coupling as low as  $\hbar\Omega = 25$  meV. Both the excitonic fraction and the effective mass of the lower polariton dispersion minimum decrease with detuning  $\Delta$  as shown in the inset of Fig. 4c and in Fig. 4d, respectively.

We calculate the polariton BEC transition temperature  $T_c$  for various QW widths, exciton trap sizes, detunings, and exciton-photon couplings for fixed polariton density. The results are plotted in Fig. 5. Clearly, room temperature polariton BEC is attainable at overall polariton density  $\gtrsim 3 \times 10^3 \mu\text{m}^{-2}$ . This is well below the saturation density in each QW of  $(5a_B)^{-2}$  where  $a_B$  is the exciton Bohr radius. The transition temperature is higher for smaller QW width since a larger number of QWs can be used. It is likewise higher for larger exciton-photon coupling and positive detuning. This is consistent with the picture that  $T_c$  is limited by the dispersion depth  $V$ . For large trap sizes  $D \gg 10 \mu\text{m}$ ,  $T_c$  decreases as expected from the Mermin-Wagner theorem[73] that forbids finite temperature BEC in an infinite 2D system. However, this decrease is very slow and little degradation in  $T_c$  is seen over the range of  $10 \mu\text{m} < D < 1$  cm. Interestingly the exciton trap size dependence of  $T_c$  for smaller  $D$  is nonmonotonic:  $T_c$  has a peak value around a box size  $D \simeq 5 \mu\text{m}$ . When the exciton trap size is sufficiently small, the quantization energy of the cavity (e.g., the energy difference between the first excited state and the ground state) can be comparable or larger than the dispersion depth  $V$ . The condensation then crosses over from polariton-like to exciton-like. Since the exciton effective mass is much larger than that of polariton, the transition temperature is rapidly reduced.

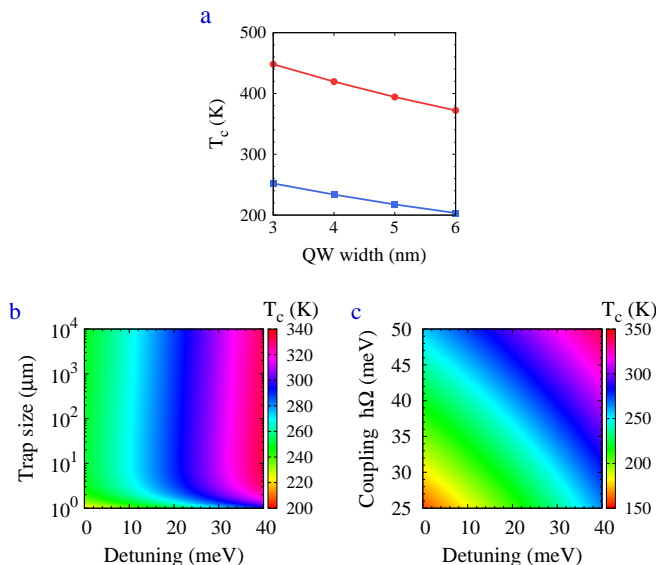


FIG. 5. Polariton BEC transition temperature  $T_c$  at fixed densities. (a) Transition temperature  $T_c$  with detuning  $\Delta = 30$  meV for different QW width (with QWs filling entire active region) at fixed polariton densities:  $1.5 \times 10^4 \mu\text{m}^{-2}$  (curve with solid circles) and  $1.9 \times 10^3 \mu\text{m}^{-2}$  (curve with solid squares). For the higher total density, the exciton density in each QW is below  $(9a_B)^{-2}$ . For the lower total density, the exciton density in each QW is below  $(26a_B)^{-2}$ . (b) Dependence of the transition temperature  $T_c$  on the detuning  $\Delta$  and the exciton trap size  $D$  when the exciton-photon coupling is  $\hbar\Omega = 48$  meV (QW width 4 nm and barrier width 5 nm) and the polariton density is  $3 \times 10^3 \mu\text{m}^{-2}$ . (c) Dependence of the transition temperature  $T_c$  on the detuning  $\Delta$  and the exciton-photon coupling  $\hbar\Omega$  when the exciton trap size is  $D = 10 \mu\text{m}$  and the polariton density is  $3 \times 10^3 \mu\text{m}^{-2}$ .

The polariton density used in our calculation is experimentally accessible. For MQWs the total exciton density is distributed among the QWs and the excitonic fraction in each QW of a polariton may be much less than unity. For example, using  $N = 100$  QWs, each of width 4 nm and barrier width 5 nm (i.e.,  $\hbar\omega_0 = 1.56$  eV and  $E_{X0} = 1.59$  eV with  $a = 365$  nm and  $a_B = 3.8$  nm), the collective exciton-photon coupling is 48 meV. For a detuning of  $\Delta = 30$  meV, the largest excitonic fraction in any single QW is 5.5% [the exciton fraction varies among QWs since the exciton-photon coupling for each QW is different, see Eq. (3)]. For total polariton density  $1.5 \times 10^4 \mu\text{m}^{-2}$ , the exciton density in each QW is no larger than  $(9a_B)^{-2}$  where  $a_B$  is the exciton Bohr radius. This single QW exciton density is less than the saturation density [28, 44]  $\simeq (5a_B)^{-2}$ .

Systematic dependence of the BEC transition temperature on total polariton density is shown in Fig. 6. Fig. 6a reveals that the exciton trap size dependence of  $T_c$  is much more pronounced at low polariton density where the transition temperature is much smaller than  $V/k_B$ . Here most polaritons are low energy photon-like states with very small effective mass. The transition tempera-

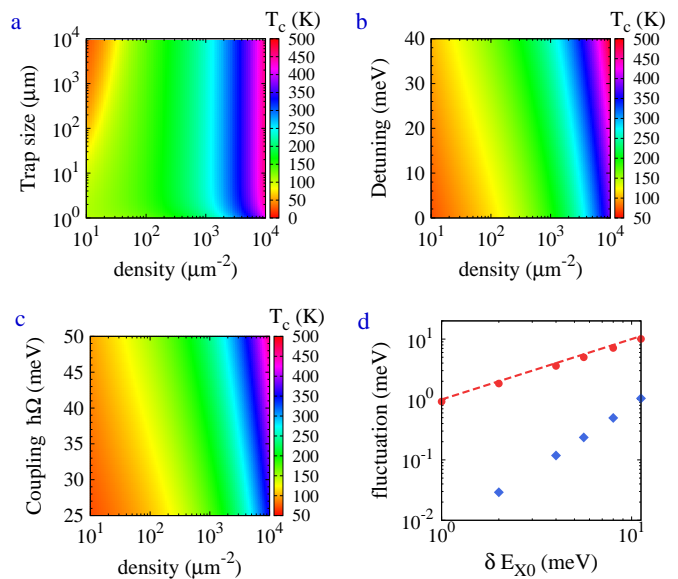


FIG. 6. BEC transition temperature  $T_c$  as a function of total polariton density and (a) box trap size, (b) exciton-photon detuning, and (c) exciton-photon coupling strength. (d) Root mean square deviation of the vacuum Rabi splitting (circles) and lower polariton dispersion depth (diamonds) as a function of exciton inhomogeneous broadening  $\delta E_{X0}$ . In (a) and (b) the exciton-photon coupling is  $\hbar\Omega = 48$  meV (QW width 4 nm and barrier width 5 nm). For (a) and (c) the detuning is 30 meV. For (b) and (c) the exciton box trap size is  $10 \mu\text{m}$ . The exciton recombination energy is  $E_{X0} = 1.59$  eV. For (d), the detuning is  $\Delta = 0$ . The dashed curve in (d) depicts the value of  $\delta E_{X0}$  itself for reference.

ture at fixed density is limited mainly by the level spacing between the ground and first excited state [18, 72], which depends sensitively on the exciton trap size. In contrast, at high polariton density, the transition temperature is close to  $V/k_B$ . When the dispersion depth  $V$  is the main factor limiting  $T_c$ , the exciton trap size has marginal influence. Figs. 6b and 6c reveal that large detuning and/or exciton-photon coupling is favorable for room temperature polariton BEC because both of them enhance the dispersion depth  $V$  (see Fig. 4d).

Finally we discuss the effect of fabrication disorder. This can randomize sensitive parameters such as the detuning  $\Delta$  and the collective exciton-photon coupling  $\hbar\Omega$ . We show that the former effect is more significant. Photonic disorder arises from fluctuation of the shape and size of the rods and slabs constituting the photonic crystal. Electronic disorder arises from impurities, dislocations, (local) QW width fluctuation, random strains, etc. In addition to these forms of inhomogeneous broadening, dynamic fluctuations (homogeneous broadening) arise from phonon-polariton and polariton-polariton interactions. These are particularly important at high temperatures.

Plane wave expansion calculation indicates that the 2D photonic band edge varies by less than 2% of its value if



the fabrication error is smaller than 20 nm for woodpile rods outside the active region, less than 12 nm for rods in the active woodpile region, and less than 6 nm for the central slab thickness. The effect of electronic disorder has been studied earlier[62] for the single QW case, where it was found that polaritons remain robust due to their small effective mass and highly mobile half-photon nature. Electronic scale disorder is largely averaged out in a scenario similar to motional narrowing[62].

For the MQW structures studied here, there are also fluctuations of exciton energy among QWs due to variations in QW width or lateral confinement of the rods. This broadening is modeled by adding a random energy  $\delta E_l$  to the exciton dispersion in the  $l$ -th QW,  $E_X^{(l)}(\vec{q}) = E_{X0} + \frac{\hbar^2 q^2}{2m_X} + \delta E_l$ .  $\delta E_l$  is modeled as a Gaussian random variable with variance  $(\delta E_{X0})^2$ . The effects of this disorder on vacuum Rabi splitting  $2\hbar\Omega$  and polariton dispersion depth  $V$  are presented in Fig. 6d. The calculation is performed by averaging over  $10^5$  random configurations. The standard deviation of the vacuum Rabi splitting is very small due to the collective nature of the polariton. The fluctuation in polariton energy consists of sum of random exciton energy variations from each of the  $N$  QWs. The total effect is an average effect which has a much smaller variance according to the central limit theorem[46],  $\frac{\delta\Omega}{\Omega} \sim \mathcal{O}\left(\frac{1}{\sqrt{N}}\right)$ .

The fluctuation of the polariton dispersion depth  $V$  is approximately the same as the inhomogeneous broadening of the exciton,  $\delta E_{X0}$ . The randomization of the detuning  $\Delta$  directly affects this dispersion depth [see Eq. (8)]. This effect is much more significant than the fluctuation of the vacuum Rabi splitting  $2\hbar\Omega$ . Experimental measurements in a single CdTe/CdMgTe QW give a typical inhomogeneous broadening of 1 meV[33]. Hence intra-QW inhomogeneous broadening can be rendered small with present-day fabrication capabilities. Inter-QW inhomogeneous broadening estimated from lateral confinement difference for QWs in rods and in the central slab is less than 1 meV as well.

Finally, dynamic fluctuations (such as polariton-phonon and polariton-polariton scattering) cause both homogeneous broadening and relaxation of polaritons. The latter is crucial for polaritons to reach the ground state and achieve thermal equilibrium BEC. However, homogeneous broadening reduces the polariton dispersion depth  $V$  and consequently  $T_c$ . In CdTe QWs, at room temperature, experiments[55] suggest a homogeneous linewidth of  $\Gamma = 22$  meV [see Appendix]. The broadening of the cavity photon is negligible for high quality factor ( $2 \times 10^6$  as shown in Ref. [53]) photonic crystal microcavities. If we estimate the effect of homogeneous broadening by adding an imaginary part,  $i\Gamma$ , to the exciton energy, the VRS at zero detuning ( $\Delta = 0$ ) is reduced to  $2\sqrt{\hbar^2\Omega^2 - \Gamma^2}/4$ [63]. More importantly, the dispersion depth of the lower polariton for nonzero de-

tuning becomes:

$$V = \frac{\Delta}{2} + \text{Re}\sqrt{\left(\frac{\Delta - i\Gamma}{2}\right)^2 + \hbar^2\Omega^2} \quad (9)$$

In general, exciton-phonon interaction reduces the dispersion depth  $V$ . However, for  $\Delta = 30$  meV,  $\hbar\Omega = 48$  meV, and  $\Gamma = 22$  meV, the lower polariton dispersion depth is reduced by only 1.1 meV. This is equivalent to a reduction of detuning by 2 meV and has negligible effects on the transition temperature according to Fig. 6b. These results suggest that our very strongly coupled exciton-photon system can withstand considerable homogeneous and inhomogeneous broadening and still deliver equilibrium room temperature polariton BEC.

## V. CONCLUSION

In summary, we have identified a CdTe-based photonic band gap architecture with a range of different quantum well embeddings that are predicted to support room temperature (or higher) equilibrium Bose-Einstein condensation of exciton-polaritons. The most crucial factors in enabling high temperature BEC are the dispersion depth of the lower polariton branch and the total areal density of long-lived excitons within the trapping region. The dispersion depth is determined by the collective exciton-photon coupling strength and is enhanced by detuning the bare exciton recombination energy above the lower edge of a slow-light, 2D guided photonic band within the larger 3D photonic band gap. The 3D PBG enables considerably stronger light trapping than conventional 1D Fabry-Pérot microcavities, leading to stronger exciton-photon coupling. The collective exciton-phonon coupling strength is further enhanced by embedding up to about 100 quantum wells in the photonic crystal regions adjacent to a central slab region containing two principal quantum wells. Positive detuning of the exciton recombination energy relative to the strongly-coupled photon mode is made possible by the 3D PBG. The positively detuned exciton remains within the 3D PBG and it cannot decay radiatively into extraneous optical modes that leave the system.

The total areal density of excitons is enhanced by distributing them over a large number of quantum wells that are all strongly coupled to the 2D guided mode within the 3D PBG. The use of CdTe-based architectures offers a suitable balance between photonic and electronic properties. The relatively low dielectric constant of CdTe compared to other popular materials (such as GaAs) enables a small exciton Bohr radius and higher saturation exciton density. Nevertheless, the dielectric constant is sufficiently large to facilitate a 3D PBG that encompasses the lower polariton dispersion depth and provides strong 3D light confinement.

Our calculations of the BEC transition temperature are based on a non-interacting polariton gas confined

in a 2D box trap. Previous studies[18] have shown that a slight reduction in the BEC transition, together with polariton anti-bunching effects are expected when exciton-exciton interactions are included in the microscopic Hamiltonian. While a box trap of  $5\ \mu\text{m}$  side length is predicted to yield the highest BEC transition temperature, very little degradation of  $T_c$  is seen for box dimensions up to 1 cm when polariton density is high. This suggests that BEC may be observable in a finite-size photonic crystal up to centimeter-scale lateral dimension, without recourse to a separately engineered 2D trap.

It is significant that for total polariton densities approaching  $10^4\ \mu\text{m}^{-2}$ , the exciton density per quantum well remains below  $(10a_B)^{-2}$ , where  $a_B$  is the exciton Bohr radius. At these densities, our PBG architecture provides sufficiently strong exciton-photon coupling and polariton dispersion depth to provide a predicted BEC transition as high as 500 K, in the absence of additional homogeneous and inhomogeneous broadening effects. This offers a safe margin for the realization of room temperature BEC in realistic systems with both foreseen and unforeseen fabrication imperfections, exciton-phonon scattering processes and other damping effects. In this way, the photonic band gap architecture provides a realistic prospect of bringing the magic of macroscopic quantum mechanics to the realm of everyday experience.

## ACKNOWLEDGMENTS

This work was supported by the Natural Sciences and Engineering Research Council of Canada, the Canadian Institute for Advanced Research, and the United States Department of Energy Contract No. DE-FG02-10ER46754.

## Appendix A: Calculation Methods and Details

The spectrum and wavefunction of the photonic bands are calculated by solving the Maxwell equations using the plane wave expansion method[60]. In calculating the photonic bands in  $\text{Cd}_{0.4}\text{Mg}_{0.6}\text{Te}/\text{Cd}_{0.8}\text{Mn}_{0.2}\text{Te}$  Fabry-Pérot cavity the dielectric constants for  $\text{Cd}_{0.4}\text{Mg}_{0.6}\text{Te}$  is 7.0 (linear interpolation between the dielectric constant of CdTe, 8.5[49], and that of MgTe, 6.0[50]) while the dielectric constant of  $\text{Cd}_{0.8}\text{Mn}_{0.2}\text{Te}$  is 7.8[74]. The electronic structures are calculated using the effective mass approximation[45]. The effective mass of the electron is  $m_e = 0.095m_0$  with  $m_0$  being the bare electron mass in vacuum[58]. For the [001]-grown QWs concerned in this work, the heavy-hole effective mass along the growth direction is  $0.6m_0$ [75], while the effective mass in the QW plane is  $m_h = 0.4m_0$ [48]. The energy and wavefunctions of the electron and hole subbands are calculated using a finite-depth well model[45]. The electronic band gap of CdTe is  $E_g = 1.475\ \text{eV}$ [58, 76], while the electronic band gap for MgTe is  $3.49\ \text{eV}$ [77]. Linear interpolation yields the band gap of  $\text{Cd}_{0.6}\text{Mg}_{0.4}\text{Te}$  as  $2.28\ \text{eV}$ . The band gap

difference between  $\text{Cd}_{0.6}\text{Mg}_{0.4}\text{Te}$  and CdTe is  $0.8\ \text{eV}$ . The offset for the conduction band between those two materials is 70% of their band gap difference[78]. The interband dipole matrix element is given by

$$d = \frac{e\hbar\sqrt{E_{cv}}}{E_g\sqrt{2m_0}}, \quad (\text{A1})$$

where  $E_{cv} = 2P_{cv}^2/m_0$  is the energy related to the momentum matrix element,  $P_{cv}$ , between the conduction and valence bands. From Ref. [78] we take  $E_{cv} = 21\ \text{eV}$ . Material parameters in the above are taken for room temperature.

The exciton spectrum and wavefunctions are calculated by diagonalizing the exciton Hamiltonian. For our narrow QWs, we consider only the excitons formed by electrons and holes in their lowest subband[43]. We ignore the mixing with higher subbands and diagonalize the exciton Hamiltonian within the lowest subband numerically. This calculation yields an exciton binding energy comparable to the experimentally observed one. The exciton wave amplitude  $|\phi(0)|$  and exciton Bohr radius are also obtained, using the same considerations.

The Auger recombination time,  $\tau_A$ , is estimated using the method presented in Ref. [67]. For a volume exciton density of  $10^{17}\text{cm}^{-3}$  (volume density of excitons corresponding to an areal polariton density of  $10^4\ \mu\text{m}^{-2}$ , estimated by dividing the areal polariton density by the thickness of the active region) in CdTe,  $\tau_A \simeq 10^{-3}$  second. This very small Auger recombination rate is due to the large band gap and small carrier density. Another non-radiative decay mechanism is the Shockley-Read-Hall mechanism due to electronic trapping centers within the semiconductor band gap. However, experiments in high quality CdTe QWs have shown photoluminescence decay time of 150 ps at room temperature[54]. This places a lower bound on the non-radiative decay time.

The polariton thermalization time is estimated as follows. Experiments[55] have found that exciton homogeneous broadening at high temperature is dominated by interactions with longitudinal-optical (LO) phonons. The exciton line width is given by  $A_{LO}/[\exp(E_{LO}/k_B T) - 1]$  where  $E_{LO} = 21.3\ \text{meV}$  is the LO-phonon energy[58] and the parameter  $A_{LO} = 15\ \text{meV}$  is fitted from the measured temperature dependence of the exciton line width in Ref. [55]. Using this result, we estimate the exciton line width due to LO-phonon scattering at  $T = 300\ \text{K}$  is  $22\ \text{meV}$ . This suggests a polariton line width at zero detuning ( $\Delta = 0$ ) of  $11\ \text{meV}$  (exciton fraction of polariton is 50%) and corresponds to a sub-picosecond thermalization time. For positive detuning, if the exciton fraction in the polariton remains larger than 10%, then the thermalization time is below or around 1 picosecond. This is considerably smaller than the non-radiative decay time of polariton, and suggests that the polariton gas has sufficient time to reach thermal equilibrium.

- 
- [1] C. Weisbuch, M. Nishioka, A. Ishikawa, and Y. Arakawa, *Observation of the coupled exciton-photon mode splitting in a semiconductor quantum microcavity*, Phys. Rev. Lett. **69**, 3314 (1992).
- [2] G. Khitrova, H. M. Gibbs, M. Kira, S. W. Koch, and A. Scherer, *Vacuum Rabi splitting in semiconductors*, Nature Phys. **2**, 81 (2006).
- [3] *The Physics of Semiconductor Microcavities*, edited by B. Deveaud (Wiley-VCH, Weinheim, 2007).
- [4] H. Deng, H. Haug, and Y. Yamamoto, *Exciton-polariton Bose-Einstein condensation*, Rev. Mod. Phys. **82**, 1489 (2010).
- [5] I. Carusotto and C. Ciuti, *Quantum fluids of light*, Rev. Mod. Phys. **85**, 299 (2013).
- [6] H. Deng, G. Weihs, C. Santori, J. Bloch, Y. Yamamoto, *Condensation of Semiconductor Microcavity Exciton Polaritons*, Science **298**, 199 (2002).
- [7] H. Deng, G. Weihs, D. Snoke, J. Bloch, and Y. Yamamoto, *Polariton lasing vs. photon lasing in a semiconductor microcavity*, Proc. Natl. Acad. Sci. U.S.A. **100**, 15318 (2003).
- [8] J. Kasprzak, M. Richard, S. Kundermann, A. Baas, P. Jeambrun, J. M. J. Keeling, F. M. Marchetti, M. H. Szymaska, R. André, J. L. Staehli, V. Savona, P. B. Littlewood, B. Deveaud, and L. S. Dang, *Bose-Einstein condensation of exciton polaritons*, Nature **443**, 409 (2006).
- [9] R. Balili, V. Hartwell, D. Snoke, L. Pfeiffer, K. West, *Bose-Einstein Condensation of Microcavity Polaritons in a Trap*, Science **316**, 1007 (2007).
- [10] A. Amo, J. Lefrère, S. Pigeon, C. Adrados, C. Ciuti, I. Carusotto, R. Houdré, E. Giacobino, and A. Bramati, *Superfluidity of polaritons in semiconductor microcavities*, Nature Phys. **5**, 805 (2009).
- [11] K. G. Lagoudakis, M. Wouters, M. Richard, A. Baas, I. Carusotto, R. André, L. S. Dang, and B. Deveaud-Plédran, *Quantized vortices in an excitonpolariton condensate*, Nature Phys. **4**, 706 (2008); D. Sanvitto, F. M. Marchetti, M. H. Szymańska, G. Tosi, M. Baudisch, F. P. Laussy, D. N. Krizhanovskii, M. S. Skolnick, L. Marrucci, A. Lemaître, J. Bloch, C. Tejedor, and L. Viña, *Persistent currents and quantized vortices in a polariton superfluid*, Nature Phys. **6**, 527 (2010); K. G. Lagoudakis, T. Ostatnický, A. V. Kavokin, Y. G. Rubo, R. André, and B. Deveaud-Plédran, *Observation of Half-Quantum Vortices in an Exciton-Polariton Condensate*, Science **326**, 974 (2009).
- [12] C. W. Lai, N. Y. Kim, S. Utsunomiya, G. Roumpos, H. Deng, M. D. Fraser, T. Byrnes, P. Recher, N. Kumada, T. Fujisawa, and Y. Yamamoto, *Coherent zero-state and  $\pi$ -state in an exciton-polariton condensate array*, Nature **450**, 529 (2007).
- [13] A. Amo, S. Pigeon, D. Sanvitto, V. G. Sala, R. Hivet, I. Carusotto, F. Pisanello, G. Leménager, R. Houdré, E. Giacobino, C. Ciuti, and A. Bramati, *Polariton Superfluids Reveal Quantum Hydrodynamic Solitons*, Science **332**, 1167-1170 (2011).
- [14] L. V. Butov and A. V. Kavokin, *The behaviour of exciton-polaritons*, Nature Photon. **6**, 2 (2012); B. Deveaud-Plédran, Nature Photon. **6**, 205 (2012).
- [15] B. Nelsen, G. Liu, M. Steger, D. W. Snoke, R. Balili, K. West, and L. Pfeiffer, *Dissipationless Flow and Sharp Threshold of a Polariton Condensate with Long Lifetime*, Phys. Rev. X **3**, 041015 (2013); M. Steger, G. Liu, B. Nelsen, C. Gautham, D. W. Snoke, R. Balili, L. Pfeiffer, and K. West, *Long-range ballistic motion and coherent flow of long-lifetime polaritons*, Phys. Rev. B **88**, 235314 (2013).
- [16] A. Imamoglu, R. J. Ram, S. Pau, and Y. Yamamoto, *Nonequilibrium condensates and lasers without inversion: Exciton-polariton lasers*, Phys. Rev. A **53**, 4250 (1996).
- [17] C. Schneider, A. Rahimi-Iman, N. Y. Kim, J. Fischer, I. G. Savenko, M. Amthor, M. Lermer, A. Wolf, L. Worschech, V. D. Kulakovskii, I. A. Shelykh, M. Kamp, S. Reitzenstein, A. Forchel, Y. Yamamoto, and S. Höfling, *An electrically pumped polariton laser*, Nature **497**, 348 (2013); P. Bhattacharya, B. Xiao, A. Das, S. Bhowmick, and J. Heo, *Solid State Electrically Injected Exciton-Polariton Laser*, Phys. Rev. Lett. **110**, 206403 (2013).
- [18] S. J. Yang and S. John, *Coherence and antibunching in a trapped interacting Bose-Einstein condensate*, Phys. Rev. B **84**, 024515 (2011).
- [19] D. Ballarini, M. De Giorgi, E. Cancellieri, R. Houdré, E. Giacobino, R. Cingolani, A. Bramati, G. Gigli, and D. Sanvitto, *All-optical polariton transistor*, Nat. Commun. **4**, 1778 (2013).
- [20] H. S. Nguyen, D. Vishnevsky, C. Sturm, D. Tanese, D. Solnyshkov, E. Galopin, A. Lemaître, I. Sagnes, A. Amo, G. Malpuech, and J. Bloch, *Realization of a Double-Barrier Resonant Tunneling Diode for Cavity Polaritons*, Phys. Rev. Lett. **110**, 236601 (2013).
- [21] S. John and T. Quang, *Collective Switching and Inversion without Fluctuation of Two-Level Atoms in Confined Photonic Systems*, Phys. Rev. Lett. **78**, 1888-1891 (1997).
- [22] A. Amo, T. C. H. Liew, C. Adrados, R. Houdré, E. Giacobino, A. V. Kavokin, and A. Bramati, *Exciton-polariton spin switches*, Nature Photon. **4**, 361-366 (2010); R. Cerna, Y. Léger, T. K. Paraiso, M. Wouters, F. Morier-Genoud, M. T. Portella-Oberli, and B. Deveaud, *Ultrafast tristable spin memory of a coherent polariton gas*, Nat. Commun. **4**, 2008 (2013).
- [23] A. Kavokin, *Polaritons: the rise of the bosonic laser*, Nature Photon. **7**, 591-592 (2013); D. Snoke, *Microcavity polaritons: A new type of light switch*, Nature Nanotech. **8**, 393-395 (2013).
- [24] S. Christopoulos, G. Baldassarri H. von Högersthal, A. J. D. Grundy, P. G. Lagoudakis, A. V. Kavokin, J. J. Baumberg, G. Christmann, R. Butté, E. Feltin, J.-F. Carlin, and N. Grandjean *Room-Temperature Polariton Lasing in Semiconductor Microcavities*, Phys. Rev. Lett. **98**, 126405 (2007); Gabriel Christmann, R. Butté, Eric Feltin, J.-F. Carlin, and Nicolas Grandjean, *Room temperature polariton lasing in a GaN/AlGaIn multiple quantum well microcavity*, Appl. Phys. Lett. **93**, 051102 (2008).
- [25] Ying-Yu Lai, Yu-Pin Lan and Tien-Chang Lu, *Strong light-matter interaction in ZnO microcavities*, Light: Science & Applications **2**, e76 (2013)
- [26] F. Li et al., *From Excitonic to Photonic Polariton Condensate in a ZnO-Based Microcavity*, Phys. Rev. Lett. **110**, 196406 (2013).

- [27] D. G. Lidzey, D. D. C. Bradley, T. Virgili, A. Armitage, M. S. Skolnick, and S. Walker, *Room Temperature Polariton Emission from Strongly Coupled Organic Semiconductor Microcavities*, Phys. Rev. Lett. **82**, 3316 (1999); S. Kéna-Cohen and S. R. Forrest, *Room-temperature polariton lasing in an organic single-crystal microcavity*, Nature Photon. **4**, 371 (2010).
- [28] S. Schmitt-Rink, D. S. Chemla, and D. A. B. Miller, *Theory of transient excitonic optical nonlinearities in semiconductor quantum-well structures*, Phys. Rev. B **32**, 6601 (1985).
- [29] R. Butté, G. Christmann, E. Feltin, J.-F. Carlin, M. Mosca, M. Ilegems, and N. Grandjean, *Room-temperature polariton luminescence from a bulk GaN microcavity*, Phys. Rev. B **73**, 033315 (2006).
- [30] R. Schmidt-Grund, B. Rheinländer, C. Czekalla, G. Bendorf, H. Hochmuth, M. Lorenz, and M. Grundmann, *Exciton-polariton formation at room temperature in a planar ZnO resonator structure*, Appl. Phys. B **93**, 331 (2008).
- [31] G. Christmann, R. Butté, E. Feltin, A. Mouti, P. A. Stadelmann, A. Castiglia, J.-F. Carlin, and N. Grandjean, *Large vacuum Rabi splitting in a multiple quantum well GaN-based microcavity in the strong-coupling regime*, Phys. Rev. B **77**, 085310 (2008).
- [32] J.-R. Chen, T.-C. Lu, Y.-C. Wu, S.-C. Lin, W.-R. Liu, W.-F. Hsieh, C.-C. Kuo, and C.-C. Lee, *Large vacuum Rabi splitting in ZnO-based hybrid microcavities observed at room temperature*, Appl. Phys. Lett. **94**, 061103 (2009).
- [33] G. V. Astakhov, V. A. Kosobukin, V. P. Kochereshko, D. R. Yakovlev, W. Ossau, G. Landwehr, T. Wojtowicz, G. Karczewski, and J. Kossut, *Inhomogeneous broadening of exciton lines in magneto-optical reflection from CdTe/CdMgTe quantum wells*, Eur. Phys. J. B **24**, 7-13 (2001).
- [34] J. Klaers, J. Schmitt, F. Vewinger, and M. Weitz, *Bose-Einstein condensation of photons in an optical microcavity*, Nature **468**, 545 (2010).
- [35] J. Schmitt, T. Damm, D. Dung, F. Vewinger, J. Klaers, and M. Weitz, *Observation of Grand-Canonical Number Statistics in a Photon Bose-Einstein Condensate*, Phys. Rev. Lett. **112**, 030401 (2014); J. Klaers, J. Schmitt, T. Damm, F. Vewinger, and M. Weitz, *Bose-Einstein condensation of paraxial light*, Appl. Phys. B **105**, 17 (2011).
- [36] D. W. Snoke, *Polariton Condensation and Lasing*, in *Exciton Polaritons in Microcavities* (Springer Series in Solid State Sciences **172**), V. Timofeev and D. Sanvitto, eds. (Springer, 2012).
- [37] S. John, *Strong localization of photons in certain disordered dielectric superlattices*, Phys. Rev. Lett. **58**, 2486 (1987).
- [38] E. Yablonoitch, *Inhibited Spontaneous Emission in Solid-State Physics and Electronics*, Phys. Rev. Lett. **58**, 2059 (1987).
- [39] O. Painter, R. K. Lee, A. Scherer, A. Yariv, J. D. O'Brien, P. D. Dapkus, and I. Kim, *Two-Dimensional Photonic Band-Gap Defect Mode Laser*, Science **284**, 1819 (1999).
- [40] S. Ogawa, M. Imada, S. Yoshimoto, M. Okano, and S. Noda, *Control of Light Emission by 3D Photonic Crystals*, Science **305**, 227 (2004); S. Noda, M. Fujita, and T. Asano, *Spontaneous-emission control by photonic crystals and nanocavities*, Nature Photon. **1**, 449 (2007).
- [41] K. Hennessy, A. Badolato, M. Winger, D. Gerace, M. Atatüre, S. Gulde, S. Fält, E. L. Hu, and A. Imamoglu, *Quantum nature of a strongly coupled single quantum dot-cavity system*, Nature **445**, 896 (2007).
- [42] S. R. Jackson, J. E. Nicholls, W. E. Hagston, P. Harrison, T. Stirner, J. H. C. Hogg, B. Lunn, and D. E. Ashenford, *Magneto-optical study of excitonic binding energies, band offsets, and the role of interface potentials in CdTe/Cd<sub>1-x</sub>Mn<sub>x</sub>Te multiple quantum wells*, Phys. Rev. B **50**, 5392 (1994).
- [43] R. André, D. Heger, L. S. Dang, and Y. M. d'Aubigné, *Spectroscopy of polaritons in CdTe-based microcavities*, J. Cryst. Growth. **184/185**, 758-762 (1998).
- [44] L. S. Dang, D. Heger, R. André, F. Boeuf, and R. Romestain, *Stimulation of Polariton Photoluminescence in Semiconductor Microcavity*, Phys. Rev. Lett. **81**, 3920 (1998).
- [45] P. Harrison, *Quantum Wells, Wires and Dots* (Wiley, New York, 2001).
- [46] J.-H. Jiang and S. John, to be published.
- [47] S. Faure, T. Guillet, P. Lefebvre, T. Bretagnon, and B. Gil, *Comparison of strong coupling regimes in bulk GaAs, GaN, and ZnO semiconductor microcavities*, Phys. Rev. B **78**, 235323 (2008).
- [48] P. Harrison, F. Long, and W. E. Hagston, *Empirical pseudo-potential calculation of the in-plane effective masses of electron and holes of two-dimensional excitons in CdTe quantum wells*, Superlattices and Microstructures, **19**, 123 (1996).
- [49] D. T. F. Marple and H. Ehrenreich, *Dielectric Constant Behavior Near Band Edges in CdTe and Ge*, Phys. Rev. Lett. **8**, 87 (1962).
- [50] *Handbook on Physical Properties of Semiconductors*, Vol. **3**, p.62, ed. S. Adachi (Kluwer Academic, Boston, 2004).
- [51] S. Noda, K. Tomoda, N. Yamamoto, and A. Chutinan, *Full Three-Dimensional Photonic Bandgap Crystals at Near-Infrared Wavelengths*, Science **289**, 604 (2000); S. Noda, M. Imada, M. Okano, S. Ogawa, M. Mochizuki, and A. Chutinan, *Semiconductor Three-Dimensional and Two-Dimensional Photonic Crystals and Devices*, IEEE J. Quantum Electron. **38**, 726 (2002).
- [52] S. Noda, N. Yamamoto, H. Kobayashi, M. Okano, and K. Tomoda, *Optical properties of three-dimensional photonic crystals based on III-V semiconductors at infrared to near-infrared wavelengths*, Appl. Phys. Lett. **75**, 905 (1999).
- [53] Y. Takahashi, H. Hagino, Y. Tanaka, B.-S. Song, T. Asano, and S. Noda, *High-Q nanocavity with a 2-ns photon lifetime*, Opt. Express **15**, 17206 (2007).
- [54] M. O'Neill, M. Oestreich, W. W. Rühle, and D. E. Ashenford, *Exciton radiative decay and homogeneous broadening in CdTe/Cd<sub>0.85</sub>Mn<sub>0.15</sub>Te multiple quantum wells*, Phys. Rev. B **48**, 8980 (1993).
- [55] R. André, F. Boeuf, D. Heger, L. S. Dang, R. Romestain, J. Bleuse, and M. Müller, *Cavity-polariton effects in II-VI microcavities*, Acta Physica Polonica A, **96**, 511 (1999).
- [56] E. Nelson et al., *Epitaxial growth of three-dimensionally architecture optoelectronic devices*, Nature Mater. **10**, 676 (2011).
- [57] T. J. Kim, Y. D. Kim, and J. Kossut, *Study on the Dielectric Function of the CdMgTe Alloy by Using Vacuum Ultraviolet Spectroscopic Ellipsometry*, J. Korean Phys. Soc. **49**, 1156 (2006).

- [58] O. Madelung, *Semiconductors: Data Handbook*, 3rd ed. (Springer, Berlin, 2004).
- [59] M. S. Dresselhaus, G. Dresselhaus, and A. Jorio, *Applications of Group Theory to the Physics of Solids*, 1st ed. (Springer, 2008).
- [60] We used the MIT photonic bands package to do the calculation. See [http://ab-initio.mit.edu/wiki/index.php/MIT\\_Photonic\\_Bands](http://ab-initio.mit.edu/wiki/index.php/MIT_Photonic_Bands)
- [61] S. John and S. J. Yang, *Electromagnetically Induced Exciton Mobility in a Photonic Band Gap*, Phys. Rev. Lett. **99**, 046801 (2007).
- [62] S. J. Yang and S. John, *Exciton dressing and capture by a photonic band edge*, Phys. Rev. B **75**, 235332 (2007).
- [63] V. Savona, L. C. Andreani, P. Schwendimann, A. Quattropani, *Quantum Well Excitons in Semiconductor Microcavities: Unified Treatment of Weak and Strong Coupling Regimes*, Solid State Commun. **93**, 733 (1995).
- [64] B. Kuhn-Heinrich, W. Ossau, H. Heinke, F. Fischer, T. Litz, A. Waag, and G. Landwehr, *Optical investigation of confinement and strain effects in CdTe/(CdMg)Te quantum wells*, Appl. Phys. Lett. **63**, 2932 (1993).
- [65] R. Spiegel, G. Bacher, K. Herz, A. Forchel, T. Litz, A. Waag, and G. Landwehr, *Recombination and thermal emission of excitons in shallow CdTe/Cd<sub>1-x</sub>Mg<sub>x</sub>Te quantum wells*, Phys. Rev. B **53**, 4544 (1996).
- [66] O. Toader, M. Berciu, and S. John, *Photonic Band Gaps Based on Tetragonal Lattices of Slanted Pores*, Phys. Rev. Lett. **90**, 233901 (2003); O. Toader and S. John, *Slanted-pore photonic band-gap materials*, Phys. Rev. E **71**, 036605 (2005).
- [67] M. A. Kinch, M. J. Brau, and A. Simmons, *Recombination mechanisms in 8-14  $\mu$  HgCdTe*, J. Appl. Phys. **44**, 1649 (1973); J. Bajaj, S. H. Shin, J. G. Pasko, and M. Khoshnevisan, *Minority carrier lifetime in LPE Hg<sub>1-x</sub>Cd<sub>x</sub>Te*, J. Vac. Sci. Tech. A **1**, 1749 (1983).
- [68] W. Shockley and W. T. Read, Jr., *Statistics of the Recombinations of Holes and Electrons*, Phys. Rev. **87**, 835 (1952); R. N. Hall, *Electron-Hole Recombination in Germanium*, Phys. Rev. **87**, 387 (1951);
- [69] T. K. Paraiso, M. Wouters, Y. Léger, F. Morier-Genoud, and B. Deveaud-Pédran, *Multistability of a coherent spin ensemble in a semiconductor microcavity*, Nature Mater. **9**, 655 (2010).
- [70] A. Das, P. Bhattacharya, J. Heo, A. Banerjee, and W. Guo, *Polariton Bose-Einstein condensate at room temperature in an Al(Ga)N nanowire-dielectric microcavity with a spatial potential trap*, Proc. Natl. Acad. Sci. USA **110**, 2735 (2013).
- [71] O. Penrose and L. Onsager, *Bose-Einstein Condensation and Liquid Helium*, Phys. Rev. **104**, 576 (1956).
- [72] W. Ketterle and N. J. van Druten, *Bose-Einstein condensation of a finite number of particles trapped in one or three dimensions*, Phys. Rev. A **54**, 656 (1996).
- [73] N. D. Mermin and H. Wagner, *Absence of Ferromagnetism or Antiferromagnetism in One- or Two-Dimensional Isotropic Heisenberg Models*, Phys. Rev. Lett. **17**, 1133 (1966).
- [74] L. Safonova, R. Brazis, and R. Narkowicz, *Complex Dielectric Constant of Cd<sub>0.8</sub>Mn<sub>0.2</sub>Te Crystals Near the Fundamental Absorption Edge*, Lith. J. Phys. **44**, 421 (2004).
- [75] L. S. Dang, G. Neu, and R. Romestain, *Optical detection of cyclotron resonance of electron and holes in CdTe*, Solid State Commun. **44**, 1187 (1982).
- [76] S. G. Choi, Y. D. Kim, S. D. Yoo, D. E. Aspnes, I. Miotkowski, and A. K. Ramdas, *Ellipsometric studies Cd<sub>1-x</sub>Mg<sub>x</sub>Te (0  $\leq$  x  $\leq$  0.5) alloys*, Appl. Phys. Lett. **71**, 249 (1997).
- [77] J.-H. Yang, S. Chen, W.-J. Yin, X. G. Gong, A. Walsh, and S.-H. Wei, *Electronic structure and phase stability of MgTe, ZnTe, CdTe, and their alloys in the B3, B4, and B8 structures*, Phys. Rev. B **79**, 245202 (2009).
- [78] A. A. Kiselev, E. L. Ivchenko, A. A. Sirenko, T. Ruf, M. Cardona, D. R. Yakovlev, W. Ossau, A. Waag, and G. Landwehr, *Electron and hole g factor anisotropy in CdTe/CdMgTe quantum wells*, J. Cryst. Growth. **184/185**, 831 (1998).